

Systematic twist expansion of $(\eta_c, \eta_b) \rightarrow \gamma^* \gamma$ transition form factors in light-front quark model

Hui-Young Ryu,¹ Ho-Meoyng Choi,^{2,*} and Chueng-Ryong Ji³

¹Department of Physics, Pusan National University, Pusan, Korea 46241

²Department of Physics, Teachers College, Kyungpook National University, Daegu, Korea 41566

³Department of Physics, North Carolina State University, Raleigh, NC 27695-8202

The light-front quark model analysis of the meson-photon transition form factor $F_{P\gamma}(Q^2)$ amenable both for the spacelike region ($Q^2 > 0$) and the timelike region ($Q^2 < 0$) provides a systematic twist expansion of $Q^2 F_{P\gamma}(Q^2)$ for the high $|Q^2|$ region. Investigating $F_{P\gamma}(Q^2)$ ($P = \eta_c, \eta_b$) for the entire kinematic regions of Q^2 , we examine the twist-2 and twist-3 distribution amplitudes of (η_c, η_b) mesons in the light-front quark model and quantify their contributions to $Q^2 F_{(\eta_c, \eta_b)\gamma}(Q^2)$. Our numerical results for the normalized transition form factor $F_{(\eta_c, \eta_b)\gamma}(Q^2)/F_{(\eta_c, \eta_b)\gamma}(0)$ and the decay width $\Gamma_{(\eta_c, \eta_b) \rightarrow \gamma\gamma}$ are compared with the available data checking the sensitivity of our model to the variation of the constituent quark masses.

I. INTRODUCTION

The pseudoscalar meson (P) production processes via the two-photon collision, $\gamma^* \gamma \rightarrow P$, involve only one transition form factor (TFF) $F_{P\gamma}(Q^2)$, where $q^2 = -Q^2$ is the squared momentum transfer of the virtual photon. This meson-photon transition is well known to be the simplest exclusive process in testing the quantum chromodynamics (QCD) and understanding the structure of the meson.

For the pseudoscalar mesons composed of the light (u, d, s) quarks such as (π^0, η, η') , there have been many experimental data for spacelike regions ($Q^2 > 0$) up to $Q^2 \sim 40 \text{ GeV}^2$ [1–6]. Especially, for the high Q^2 , the TFFs can be calculated asymptotically at leading twist as a convolution of the perturbative hard scattering amplitude and the nonperturbative meson distribution amplitude (DA) [7–9]. One of the prominent features of the perturbative QCD (pQCD) is that the TFFs show the asymptotic behaviors, $Q^2 F_{(\pi, \eta, \eta')\gamma}(Q^2) \rightarrow \text{constant}$ as $Q^2 \rightarrow \infty$. However, the results $Q^2 F_{\pi\gamma}(Q^2)$ from the BaBar Collaboration [5] are not only inconsistent with pQCD prediction but also show the rapid growth of $Q^2 F_{\pi\gamma}(Q^2)$ for $Q^2 > 15 \text{ GeV}^2$ while the measurement from Belle Collaboration [4] are consistent with the asymptotic limit of QCD for $Q^2 > 15 \text{ GeV}^2$. On the other hand, the subsequent BaBar data [6] for $Q^2 F_{(\eta, \eta')\gamma}(Q^2)$ provided a consistency with the pQCD prediction unlike the case of $Q^2 F_{\pi\gamma}(Q^2)$. These discrepancies for the results of $Q^2 F_{\pi\gamma}(Q^2)$ between the BaBar and the Belle data as well as for the different behaviors of the results between $Q^2 F_{\pi\gamma}(Q^2)$ and $Q^2 F_{(\eta, \eta')\gamma}(Q^2)$ for the high Q^2 region have motivated many theoretical studies [10–22] to investigate the key issues for the resolution of discrepancies.

To examine the issue of the scaling behavior of $Q^2 F_{P\gamma}(Q^2)$ in the large Q^2 , it may be necessary to analyze the corresponding form factor not only in the spacelike region but also in the timelike region. While there have been some theoretical analysis [23, 24] for the timelike region below the resonance value $q^2 = m_P^2$ of meson P with the physical mass m_P , we could not find any theoretical studies in timelike region for $q^2 > m_P^2$. The reason for the difficulty of analyzing the timelike region maybe due to the singular nature and the complexity of the timelike form factor beyond the resonance region. Nevertheless, in our recent work of the $(\pi^0, \eta, \eta') \rightarrow \gamma^* \gamma$ TFFs [25], we have developed the new method to explore the timelike region without resorting to mere analytic continuation from the spacelike region to the timelike region and analyzed the entire kinematic region (both for the timelike region and the spacelike region) using the light-front quark model (LFQM) [26–30]. Our direct calculation in timelike region shows the complete agreement not only with the analytic continuation result from the spacelike region but also with the result from the dispersion relation between the real and imaginary parts of the form factor. Our results of $Q^2 F_{(\pi, \eta, \eta')\gamma}(Q^2)$ were in good agreement with the available experimental data for low $|Q^2|$ region and also consistent with the pQCD prediction for the high $|Q^2|$ region.

In this work, we explore the heavy quarkonia $(\eta_c, \eta_b) \rightarrow \gamma\gamma^*$ transitions in both spacelike and timelike regions expanding our previous work of the $(\pi^0, \eta, \eta') \rightarrow \gamma^* \gamma$ TFFs [25]. For the charmonium case, the form factor $F_{\eta_c\gamma}(Q^2)$ was measured from BaBar collaboration [31] only in the spacelike region of $2 \text{ GeV}^2 < Q^2 < 50 \text{ GeV}^2$. There have been several theoretical studies on the TFF $F_{\eta_c\gamma}(Q^2)$ in the spacelike region using various theoretical approaches and phenomenological models such as pQCD [32, 33], lattice QCD [34, 35], non-relativistic QCD (NRQCD) [36, 37], QCD sum rules [38], LFQM [39], and covariant approach based on Dyson-Schwinger and Bethe-Salpeter (BS) equations [40]. In particular, a strong discrepancy between the NRQCD prediction [36] and the BaBar measurements has been recently resolved by applying the Principle of Maximum

*Electronic address: homyoung@knu.ac.kr

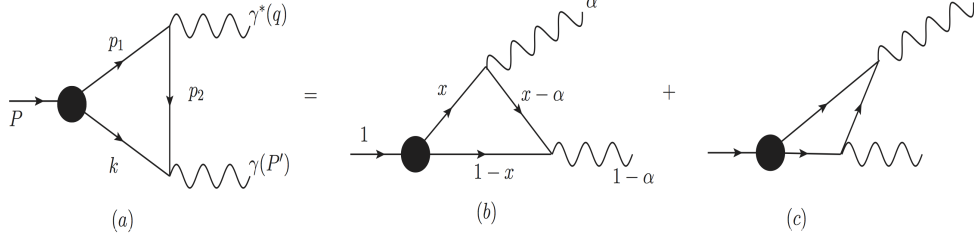


FIG. 1: One-loop Feynman diagrams that contribute to $P \rightarrow \gamma^* \gamma$. The single covariant Feynman diagram (a) is in principle the same as the sum of the two LF time-ordered diagrams (b) and (c), respectively.

Conformality to the renormalization scale [37]. Also to overcome the weakness of the Dyson-Schwinger approach caused by a series of complex-valued singularities with increasing photon-momentum square in the numerical Euclidean momentum integration, a novel method using the perturbation theory integral representations of the quark propagator, meson amplitude and quark-photon vertex has been implemented to calculate the $F_{\eta_c \gamma}(Q^2)$ for any spacelike momenta [40]. In contrast to these and other available theoretical approaches and phenomenological models, the salient feature of our LFQM analysis is to explore the timelike region as well as the spacelike region within the same theoretical framework. As we discuss in this work, the LFQM analysis of the TFF $F_{P\gamma}(Q^2)$ amenable both for the spacelike region ($Q^2 > 0$) and the timelike region ($Q^2 < 0$) provides a systematic twist expansion of $Q^2 F_{P\gamma}(Q^2)$ for the high $|Q^2|$ region.

The paper is organized as follows. In Sec. II, we briefly discuss the TFFs obtained from the $q^+ (= q^0 + q^3) \neq 0$ frame in our LFQM starting from an exactly solvable covariant BS model of (3+1)-dimensional fermion field theory. The self-consistent correspondence relations between the covariant BS model and our LFQM are also discussed and the explicit form of $F_{(\eta_c, \eta_b) \gamma}(Q^2)$ in our LFQM is presented. Especially, a systematic twist expansion of $Q^2 F_{(\eta_c, \eta_b) \gamma}(q^2)$ is provided explicitly and the leading- and higher-twist effects in the calculations of $Q^2 F_{(\eta_c, \eta_b) \gamma}(q^2)$ are discussed in this section. In Sec. III, we present our numerical results for the transverse momentum dependent distribution amplitude (TMDA), which is a 3-dimensional generalization of the DA, as well as its longitudinal and transverse moments. The $(\eta_c, \eta_b) \rightarrow \gamma^* \gamma$ TFFs for both spacelike and timelike regions are obtained and compared with the available experimental data. In order to check the validity of our LFQM calculations in the timelike regions, we verify the exact agreement of our direct LFQM calculation in the timelike region with the results obtained from the dispersion relation between the real and imaginary parts of the form factors. Conclusions follow in Sec. IV.

II. LIGHT-FRONT QUARK MODEL DESCRIPTION

The transition form factor $F_{P\gamma}$ for the $P \rightarrow \gamma^* \gamma$ ($P = \pi^0, \eta, \eta', \eta_c, \eta_b$) transition is defined from the matrix element of electromagnetic current $\Gamma^\mu = \langle \gamma(P-q) | J^\mu | P(P) \rangle$ as follows:

$$\Gamma^\mu = ie^2 F_{P\gamma}(Q^2) \varepsilon^{\mu\nu\rho\sigma} P_\nu \varepsilon_\rho q_\sigma, \quad (1)$$

where P^μ and q^μ are the four momenta of the incident pseudoscalar meson and virtual photon, respectively, and ε is the transverse polarization vector of the final (on-shell) photon. This process is illustrated by the Feynman diagram in Fig. 1 (a). In the exactly solvable manifestly covariant BS model, the covariant amplitude Γ^μ is obtained by the following momentum integral

$$\Gamma^\mu = ie_Q e_{\bar{Q}} N_c \int \frac{d^4 k}{(2\pi)^4} \frac{\text{Tr}[\gamma_5 (\not{p}_1 + m_Q) \gamma^\mu (\not{p}_2 + m_Q) \not{\varepsilon} (-\not{k} + m_Q)]}{N_{p_1} N_k N_{p_2}} H_0, \quad (2)$$

where N_c is the number of colors and $e_Q(\bar{Q})$ is the quark (antiquark) electric charge. The denominators $N_{p_j} (= p_j^2 - m_Q^2 + i\varepsilon)$ ($j = 1, 2$) and $N_k (= k^2 - m_Q^2 + i\varepsilon)$ come from the intermediate quark and antiquark propagators of mass $m_Q = m_{\bar{Q}}$ carrying the internal four-momenta $p_1 = P - k$, $p_2 = P - q - k$, and k , respectively. The $\bar{q}q$ bound-state vertex function of the meson is denoted by H_0 .

It is well known that the single covariant Feynman diagram Fig. 1 (a) is in general equal to the sum of the two LF time-ordered diagrams Figs. 1 (b) and 1(c) if the $q^+ \neq 0$ frame is taken. However, if the $q^+ = 0$ frame (but $\mathbf{q}_\perp \neq 0$ so that $q^2 = q^+ q^- - \mathbf{q}_\perp^2 = -\mathbf{q}_\perp^2 = -Q^2$) is chosen, the LF diagram 1(c) does not contribute but only the diagram 1(b) gives exactly the same result as the covariant diagram 1(a). This has been known to be the virtue of taking the $q^+ = 0$ frame in the LF calculation and many previous LF calculations have adopted this $q^+ = 0$ frame in the analysis of meson-photon TFFs [7, 21, 27, 33]. However, the analysis in the timelike region using the $q^+ = 0$ frame has been challenging since the $q^+ = 0$ frame is defined only in the spacelike region

($Q^2 > 0$) and the analytic continuation from spacelike region to timelike ($q^2 = -Q^2 > 0$) region is not quite straightforward due to the complication of mixture between the external momentum \mathbf{q}_\perp and the internal momentum \mathbf{k}_\perp included in the term showing the singularity in the timelike region as discussed in [25].

To overcome this difficulty in the analysis of the meson-photon TFFs in the timelike region, we recently explored in [25] the $q^+ \neq 0$ frames (but with $\mathbf{q}_\perp = 0$) defined in the timelike region, i.e. $\alpha = q^+/P^+ = 1 - P'^+/P^+$ frames with (1) $0 < \alpha < 1$ and (2) $\alpha = 1$. For the $0 < \alpha < 1$ case, the covariant diagram in Fig. 1 (a) is shown to be equivalent to the sum of two LF diagrams Figs. 1 (b) and 1(c). However, for the case of $\alpha = 1$, we find that Fig. 1(b) does not contribute but only Fig. 1 (c) contributes to the total transition amplitude and coincides with the covariant result of Fig. 1(a). The salient feature of the $\alpha = 1$ frame not only show the boost invariant result but also show much more effective computation of the timelike form factor over the commonly used $q^+ = 0$ (i.e. $\alpha = 0$) frame calculation [25]. By applying the self-consistent correspondence relations (see, e.g., Eq. (35) in [41]) between the covariant BS model and our LFQM found in the analysis of the twist-2 and twist-3 DAs of pseudoscalar and vector mesons [41–43] and the pion electromagnetic form factor [41], we were able to obtain the meson-photon TFFs [25] using the $\alpha = 1$ frame with the more phenomenologically accessible Gaussian wave functions backed by the LFQM analysis of meson mass spectra [26–30].

Since the TFFs for the heavy quarkonia (η_c, η_b) $\rightarrow \gamma^* \gamma$ transitions have the same form as the $F_{\pi\gamma}$ in [25] apart from the charge factor, we do not duplicate the same analysis here but display only the final form of $F_{\eta_c(\eta_b)\gamma}$ obtained from the $\alpha = 1$ frame in our LFQM:

$$F_{\eta_c(\eta_b)\gamma}(q^2) = e_{c(b)}^2 \frac{\sqrt{2N_c}}{4\pi^3} \int_0^1 \frac{dx}{(1-x)} \int d^2\mathbf{k}_\perp \frac{1}{M_0^2 - q^2} \Psi_{\frac{\uparrow\downarrow - \downarrow\uparrow}{\sqrt{2}}}(x, \mathbf{k}_\perp), \quad (3)$$

where $M_0^2 = \frac{\mathbf{k}_\perp^2 + m_Q^2}{x(1-x)}$ is the invariant mass and the LF wave function of a pseudoscalar meson with the constituent quark and antiquark mass $m_Q = m_{\bar{Q}}$ is given by

$$\Psi_{\frac{\uparrow\downarrow - \downarrow\uparrow}{\sqrt{2}}}(x, \mathbf{k}_\perp) = \frac{1}{\sqrt{2}} (\mathcal{R}_{\uparrow\downarrow}^{00} - \mathcal{R}_{\downarrow\uparrow}^{00}) \phi_{1S}(x, \mathbf{k}_\perp) = \frac{m_Q}{\sqrt{\mathbf{k}_\perp^2 + m_Q^2}} \phi_{1S}(x, \mathbf{k}_\perp), \quad (4)$$

with the spin-orbit wave function $\mathcal{R}_{\lambda_Q \lambda_{\bar{Q}}}^{J_z}$ obtained by the interaction independent Melosh transformation from the ordinary equal-time static spin-orbit wave function assigned by the quantum number J^{PC} . Explicit form of $\mathcal{R}_{\lambda_Q \lambda_{\bar{Q}}}^{00}$ for $m_Q = m_{\bar{Q}}$ case is given by

$$\mathcal{R}_{\lambda_Q \lambda_{\bar{Q}}}^{00} = \frac{1}{\sqrt{2}\sqrt{\mathbf{k}_\perp^2 + m_Q^2}} \begin{pmatrix} -k^x + ik^y & m_Q \\ -m_Q & -k^x - ik^y \end{pmatrix}, \quad (5)$$

which satisfies $\sum_{\lambda_Q \lambda_{\bar{Q}}} \mathcal{R}_{\lambda_Q \lambda_{\bar{Q}}}^{00\dagger} \mathcal{R}_{\lambda_Q \lambda_{\bar{Q}}}^{00} = 1$. For the radial wave function, we use in this work the 1S state harmonic oscillator wave function

$$\phi_{1S}(x, \mathbf{k}_\perp) = \frac{4\pi^{3/4}}{\beta^{3/2}} \sqrt{\frac{\partial k_z}{\partial x}} e^{-\frac{\vec{k}^2}{2\beta^2}}, \quad (6)$$

where $\partial k_z / \partial x = M_0 / 4x(1-x)$ is the Jacobian of the variable transformation $\{x, \mathbf{k}_\perp\} \rightarrow \vec{k} = (\mathbf{k}_\perp, k_z)$ and β is the variational parameter fixed by our previous analysis of meson mass spectra [26, 28–30]. In particular, \vec{k}^2 is given by $\vec{k}^2 = \mathbf{k}_\perp^2 + k_z^2$ where $k_z = (x - 1/2)M_0$. The normalization of ϕ_{1S} is thus given by

$$\int_0^1 dx \int \frac{d^2\mathbf{k}_\perp}{16\pi^3} |\phi_{1S}(x, \mathbf{k}_\perp)|^2 = 1. \quad (7)$$

We should note that the TFF in the $q^+ = 0$ frame is obtained by the following replacement of the denominator factor, $(M_0^2 - q^2)^{-1} \rightarrow [M_0'^2]^{-1}$ in Eq. (3), where $M_0' = M_0(\mathbf{k}_\perp \rightarrow \mathbf{k}_\perp + (1-x)\mathbf{q}_\perp)$ (see [25] for more detailed derivation). Compared to the pole structure $[M_0'^2]^{-1}$ in the timelike region of the $q^+ = 0$ frame, the internal transverse momentum \mathbf{k}_\perp for the corresponding pole structure $(M_0^2 - q^2)^{-1}$ in the $\alpha = 1$ frame as shown in Eq. (3) does not mix with the external virtual photon momentum q . Because of this salient feature for the $\alpha = 1$ frame, the direct timelike TFF calculation can be done most effectively in contrast to the computation in the $q^+ = 0$ frame. We have already explicitly shown in our numerical calculations [25] for the $(\pi^0, \eta, \eta') \rightarrow \gamma^* \gamma$ TFFs that our direct results of the timelike form factors given by Eq. (3) satisfy the following dispersion

TABLE I: Model parameters $(m_Q, \beta_{QQ})(Q = c, b)$ (in GeV).

Model	m_c	m_b	$\beta_{c\bar{c}}$	$\beta_{b\bar{b}}$	f_{η_c}	f_{η_b}
Set I	1.80	5.20	0.6509	1.1452	0.326	0.507
Set II	1.30	4.50	0.6509	1.1452	0.335	0.530
Exp. [44]	-	-	-	-	0.335(75)	-

relations (DR);

$$\begin{aligned}\text{Re } F(q^2) &= \frac{1}{\pi} P \int_{-\infty}^{\infty} \frac{\text{Im } F(q'^2)}{q'^2 - q^2} dq'^2, \\ \text{Im } F(q^2) &= -\frac{1}{\pi} P \int_{-\infty}^{\infty} \frac{\text{Re } F(q'^2)}{q'^2 - q^2} dq'^2,\end{aligned}\quad (8)$$

where P indicates the Cauchy principal value.

Moreover, a systematic twist expansion of $F_{\eta_c(\eta_b)\gamma}(q^2)$ is straightforwardly attained as discussed below by expanding the factor $1/(M_0^2 - q^2)$ in geometric sum for high $Q^2 = -q^2$;

$$\frac{1}{M_0^2 - q^2} = \frac{1}{M_0^2 + Q^2} = \frac{1}{Q^2(1 + \frac{M_0^2}{Q^2})} = \frac{1}{Q^2} - \frac{M_0^2}{Q^4} + \dots \quad (9)$$

With the expansion of the geometric sum given by Eq. (9), we can easily expand $Q^2 F_{\eta_c(b)\gamma}(Q^2)$ in Eq. (3) in terms of the twist-2, twist-3 DAs, etc. as follows

$$Q^2 F_{\eta_c(\eta_b)\gamma}(q^2) = e_{c(b)}^2 f_M \int_0^1 \frac{dx}{1-x} \left[2\phi_{2;M}(x) - 4\frac{m_Q}{Q^2} \mu_M \phi_{3;M}(x) + \mathcal{O}\left(\frac{1}{Q^{2n}}\right) \right], \quad (10)$$

with $n \geq 2$. The normalized twist-2 DA $\phi_{2;M}(x)$ and twist-3 DA $\phi_{3;M}(x)$ for the meson $M(= \eta_c, \eta_b)$ obtained from our LFQM are given by [41]

$$\phi_{2;M}(x) = \frac{\sqrt{2N_c}}{f_M 8\pi^3} \int d^2\mathbf{k}_\perp \Psi_{\frac{\uparrow\downarrow-\downarrow\uparrow}{\sqrt{2}}}(x, \mathbf{k}_\perp), \quad (11)$$

and

$$\phi_{3;M}(x) = \frac{\sqrt{2N_c}}{f_M \mu_M 16\pi^3} \int d^2\mathbf{k}_\perp \left(\frac{M_0^2}{m_Q} \right) \Psi_{\frac{\uparrow\downarrow-\downarrow\uparrow}{\sqrt{2}}}(x, \mathbf{k}_\perp), \quad (12)$$

where f_M is the decay constant and the normalization parameter μ_M in Eq. (12) results from quark condensate and can be fixed from the normalization of the DAs via $\int_0^1 dx \phi_{2(3);M}(x) = 1$. We should note that the twist-2 and twist-3 DAs $\phi_{2;M}$ and $\phi_{3;M}$ correspond to the axial-vector and pseudoscalar channels of a meson M , respectively, as discussed in [41]. The TFF for $\pi^0 \rightarrow \gamma\gamma^*$ can be obtained by replacing the charge factor $e_{c(b)}^2$ in Eq. (10) with $(e_u^2 - e_d^2)/\sqrt{2}$. The form factor at zero momentum transfer is related with the decay width for $P \rightarrow \gamma\gamma$ via

$$\Gamma_{P \rightarrow \gamma\gamma} = \frac{\pi}{4} \alpha^2 M_P^3 |F_{P\gamma}(0)|^2, \quad (13)$$

where α is the fine structure constant and M_P is the physical meson mass.

III. NUMERICAL RESULTS

In our numerical calculations, we use the two sets of model parameters for η_c and η_b as shown in Table I. While the Set I was obtained from the variational principle for the QCD-motivated effective Hamiltonian including the linear confining potential and the hyperfine interaction [26–30], the Set II provides the parameter sensitivity check of our LFQM to the constituent quark masses and at the same time the better fit to the experimental data for f_{η_c} [44] and $\Gamma_{\eta_c \rightarrow \gamma\gamma}$ [45]. We should note that the TFFs

are much more sensitive to the variation of the quark masses than to the variation of the β parameters.

Defining the transverse momentum dependent DA (TMDA) $\psi_{2(3);M}(x, \mathbf{k}_\perp)$ that is a 3-dimensional generalization of the twist-2(3) DA $\phi_{2(3);M}(x)$ as

$$\phi_{2(3);M}(x) = \int_0^\infty d^2\mathbf{k}_\perp \psi_{2(3);M}(x, \mathbf{k}_\perp) = \int_0^1 dy \psi_{2(3);M}(x, y), \quad (14)$$

the n th transverse moment is obtained by

$$\langle \mathbf{k}_\perp^n \rangle_{2(3);M} = \int_0^1 dx \int_0^\infty d^2\mathbf{k}_\perp \psi_{2(3);M}(x, \mathbf{k}_\perp) \mathbf{k}_\perp^n, \quad (15)$$

where $\psi_{2(3);M}(x, y)$ in Eq. (14) is obtained by changing the variable $\mathbf{k}_\perp^2 = y/(1-y)$. One can also define the expectation value of the longitudinal momentum, so-called ξ ($= 2x-1$)-moments, as follows:

$$\langle \xi^n \rangle_{2(3);M} = \int_0^1 dx; \phi_{2(3);M}(x) \xi^n. \quad (16)$$

Our results of the 2nd transverse moment corresponding to the $\psi_{2;M}(x, \mathbf{k}_\perp)$ and $\psi_{3;M}(x, \mathbf{k}_\perp)$ wave functions obtained from the Set I [Set II] are $\langle \mathbf{k}_\perp^2 \rangle_{2;\eta_c} = (866 \text{ MeV})^2 [(840 \text{ MeV})^2]$ and $\langle \mathbf{k}_\perp^2 \rangle_{3;\eta_c} = (940 \text{ MeV})^2 [(950 \text{ MeV})^2]$ for the η_c meson and $\langle \mathbf{k}_\perp^2 \rangle_{2;\eta_b} = (1.573 \text{ GeV})^2 [(1.561 \text{ GeV})^2]$ and $\langle \mathbf{k}_\perp^2 \rangle_{3;\eta_b} = (1.636 \text{ GeV})^2 [(1.640 \text{ GeV})^2]$ for the η_b meson, respectively. The 2nd ξ -moments of the twist-2 and twist-3 DAs obtained from the Set I [Set II] are $\langle \xi^2 \rangle_{2;\eta_c} = 0.0766 [0.111]$ and $\langle \xi^2 \rangle_{3;\eta_c} = 0.0859 [0.128]$ for the η_c meson and $\langle \xi^2 \rangle_{2;\eta_b} = 0.0377 [0.0471]$ and $\langle \xi^2 \rangle_{3;\eta_b} = 0.0402 [0.0510]$ for the η_b meson, respectively.

Figure 2 shows the TMDAs of $\eta_{c(b)}$ related with the twist-2 and 3 DAs compared with those of π meson obtained in our previous work [41], i.e., $\psi_{2;\pi}(x, y)$ (left panel) and $\psi_{3;\pi}(x, y)$ (right panel) for the π meson (upper panel), $\psi_{2;\eta_c}(x, y)$ (left panel) and $\psi_{3;\eta_c}(x, y)$ (right panel) for the η_c meson (middle panel), and $\psi_{2;\eta_b}(x, y)$ (left panel) and $\psi_{3;\eta_b}(x, y)$ (right panel) for the η_b meson (lower panel) obtained from the Set II, respectively. Comparing the TMDAs $\psi_{2;M}(x, y)$ related with the twist-2 DAs and $\psi_{3;M}(x, y)$ related with the twist-3 DAs, we find that $\psi_{3;M}(x, y)$ shows in general broader shape and receives higher \mathbf{k}_\perp -contributions than $\psi_{2;M}(x, y)$ regardless of the kinds of mesons $M(= \pi, \eta_c, \eta_b)$. On the other hand, as one can see from Fig. 2, $\psi_{2(3);\pi}(x, y)$ receives contributions from the end points of x for small \mathbf{k}_\perp regions more than the heavy quarkonia case. We also note that $\psi_{2(3);\eta_b}(x, y)$ not only show much narrower shapes but also receive higher \mathbf{k}_\perp -contributions than $\psi_{2(3);\eta_c}(x, y)$ and $\psi_{2(3);\pi}(x, y)$. For the case of heavy quarkonia TMDAs, the results from the Set I are qualitatively very similar to those from the Set II but show slightly narrower shape than those from the Set II due to the heavier quark masses.

The TFFs at $Q^2 = 0$ are obtained as $F_{\eta_c\gamma}(0) = 0.0374 [0.0664] \text{ GeV}^{-1}$ and $F_{\eta_b\gamma}(0) = 0.0019 [0.0026] \text{ GeV}^{-1}$ for the Set I [Set II], respectively. Using the following experimental values of $(M_{\eta_c}, M_{\eta_b}) = (2.98, 9.40) \text{ GeV}$ [45], we obtain $\Gamma_{\eta_c \rightarrow \gamma\gamma} = 1.55 [4.88] \text{ keV}$ and $\Gamma_{\eta_b \rightarrow \gamma\gamma} = 0.128 [0.239] \text{ keV}$ for the Set I [Set II], respectively. The experimental value of $F_{\eta_c\gamma}(0)$ may be obtained from the experimental data $\Gamma_{\eta_c\gamma\gamma}^{\text{exp}} = 5.1 \pm 0.4 \text{ keV}$ [45], which yields $F_{\eta_c\gamma\gamma}^{\text{exp}} = 0.067 \pm 0.0028 \text{ GeV}^{-1}$. Although our LFQM result for $F_{\eta_c\gamma}(0)$ obtained from the Set II rather than the Set I shows a good agreement with the experimental value, we should note that a recent lattice QCD result [35] of $\Gamma_{\eta_c \rightarrow \gamma\gamma} = 1.122(14) \text{ keV}$ is similar to ours obtained from the Set I.

In Fig. 3, we show the normalized $\eta_c \rightarrow \gamma\gamma^*$ transition form factor $F_{\eta_c\gamma}(Q^2)/F_{\eta_c\gamma}(0)$ obtained from the Set II for both timelike ($q^2 = -Q^2 > 0$) spacelike ($q^2 = -Q^2 < 0$) momentum transfer regions up to $|Q^2| = 70 \text{ GeV}^2$ and compare them with the available experimental data [31] for the spacelike region as well as the results obtained from the dispersion relation (DR). The dotted, dashed and solid lines in Fig. 3 represent our LFQM predictions of $\text{Re}[F_{\eta_c\gamma}(q^2)/F_{\eta_c\gamma}(0)]$, $\text{Im}[F_{\eta_c\gamma}(q^2)/F_{\eta_c\gamma}(0)]$ and $|F_{\eta_c\gamma}(q^2)/F_{\eta_c\gamma}(0)|$, respectively. We note that the spacelike region can be easily obtained by analytically continuing the momentum transfer $q^2 \rightarrow -q^2$ in the integrand of Eq. (3). As one can see from Fig. 3, our result for the spacelike Q^2 region shows a good agreement with the data. For the analysis of timelike form factor near resonance region in Fig. 3, the maximum value of $F_{\eta_c\gamma}(q^2)$ occurs at $q^2 \simeq 4m_c^2$ due to the virtual photon wave function term $1/(M_0^2 - q^2)$ in Eq. (3). The imaginary part of the form factor also starts to appear at $q^2 = 4m_c^2$. As a consistency check of our LFQM calculations for the timelike region, we also include the real (imaginary) part of the form factor obtained from the DR (denoted by $+$ (\times) data points) given by Eq. (8). As one can see, our direct results for the real and imaginary parts are in perfect agreement with the results obtained from the DR. This assures the validity of our numerical calculation in the timelike region.

In Fig. 4, we show the normalized TFFs $F_{\eta_c\gamma}(Q^2)/F_{\eta_c\gamma}(0)$ (left panel) for the spacelike ($q^2 = -Q^2 < 0$) momentum transfer region up to $Q^2 = 100 \text{ GeV}^2$ and $|Q^2 F_{\eta_c\gamma}(Q^2)|$ (right panel) for both timelike ($q^2 > 0$) and spacelike momentum transfer regions ($-500 \leq Q^2 \leq 500 \text{ GeV}^2$) and compare them with the available experimental data [31] for the spacelike region. The dashed and solid lines represent our results obtained from the Set I and II, respectively. We note that the spacelike region can be easily obtained by analytically continuing the momentum transfer $q^2 \rightarrow Q^2 (= -q^2)$ in the integrand of Eq. (3). Our results from the Set II are in good agreement with the available data not only for the normalized TFF $F_{\eta_c\gamma}(Q^2)/F_{\eta_c\gamma}(0)$ but also for the form

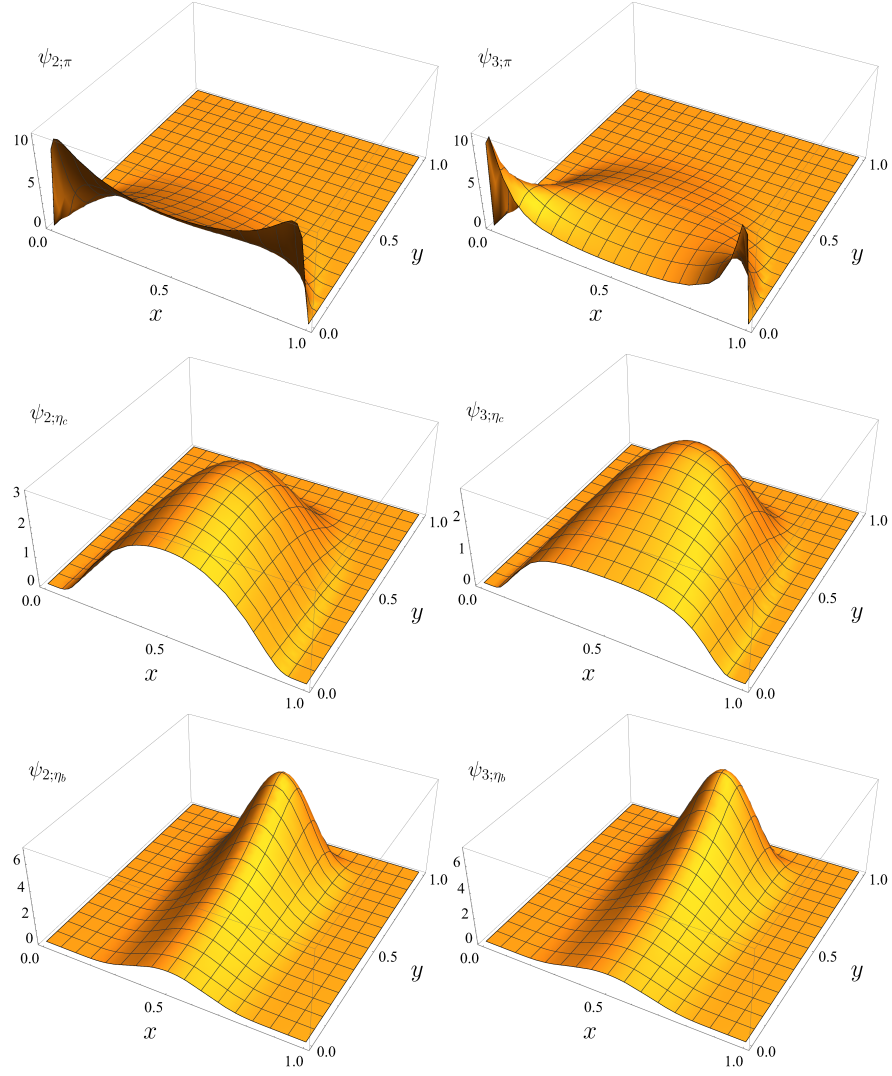


FIG. 2: Transverse momentum dependent distribution amplitudes (TMDAs) $\psi_{2;\pi}(x,y)$ (left panel) and $\psi_{3;\pi}(x,y)$ (right panel) for the π meson (upper panel), $\psi_{2;\eta_c}(x,y)$ (left panel) and $\psi_{3;\eta_c}(x,y)$ (right panel) for the η_c meson (middle panel), and $\psi_{2;\eta_b}(x,y)$ (left panel) and $\psi_{3;\eta_b}(x,y)$ (right panel) for the η_b meson (lower panel) obtained from the Set II, respectively.

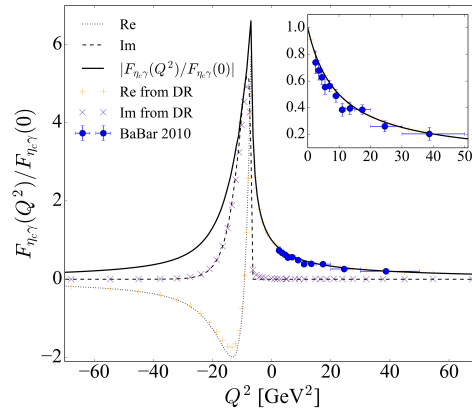


FIG. 3: The normalized $\eta_c \rightarrow \gamma\gamma^*$ transition form factor $F_{\eta_c\gamma}(Q^2)/F_{\eta_c\gamma}(0)$ obtained from the Set II for both timelike ($q^2 = -Q^2 > 0$) spacelike ($q^2 = -Q^2 < 0$) momentum transfer regions compared with the results obtained from the dispersion relation (DR). The data are taken from [31].

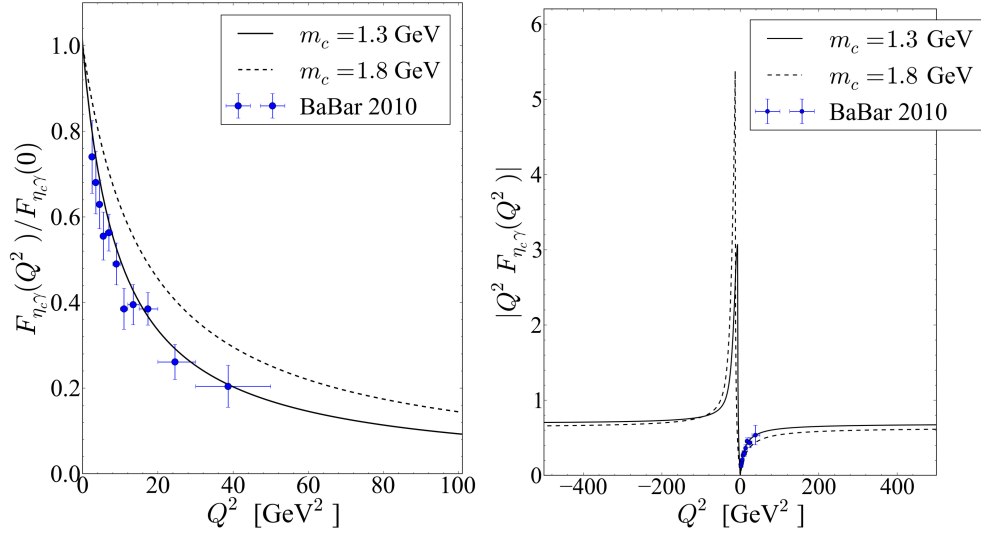


FIG. 4: The normalized $\eta_c \rightarrow \gamma\gamma^*$ transition form factor $F_{\eta_c\gamma}(Q^2)/F_{\eta_c\gamma}(0)$ in the spacelike ($q^2 = -Q^2 < 0$) momentum transfer region (left panel), and the $|Q^2 F_{\eta_c\gamma}(Q^2)|$ for both timelike ($q^2 > 0$) and spacelike momentum transfer regions (right panel). The data are taken from [31].

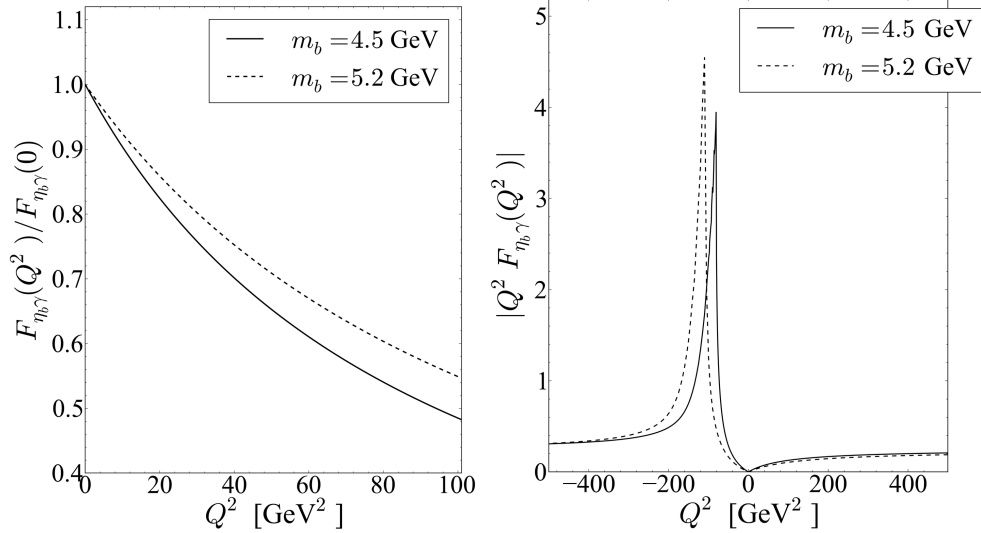


FIG. 5: The normalized $\eta_b \rightarrow \gamma\gamma^*$ transition form factor $F_{\eta_b\gamma}(Q^2)/F_{\eta_b\gamma}(0)$ in the spacelike momentum transfer region (left panel), and the $|Q^2 F_{\eta_b\gamma}(Q^2)|$ for both timelike and spacelike momentum transfer regions (right panel).

factor $F_{\eta_c\gamma}(0)$ at $Q^2 = 0$. We note that our LFQM result for $|Q^2 F_{\eta_c\gamma}(Q^2)|$ shows the asymptotic behavior for high $|Q^2|$ values, but the result in the spacelike region reaches the asymptotic value faster than that in the timelike region.

In Fig. 5, we show the normalized TFFs $F_{\eta_b\gamma}(Q^2)/F_{\eta_b\gamma}(0)$ (left panel) for the spacelike momentum transfer region up to $Q^2 = 100 \text{ GeV}^2$ and $|Q^2 F_{\eta_b\gamma}(Q^2)|$ (right panel) for both timelike and spacelike momentum transfer regions ($-500 \leq Q^2 \leq 500 \text{ GeV}^2$). The line codes are same as in Fig. 4. While the qualitative behavior of the $F_{\eta_b\gamma}$ is the same as that of $F_{\eta_c\gamma}$, their quantitative behaviors such as the slope of the form factor at $Q^2 = 0$ are quite different due to the b quark being much heavier than the c quark. Our LFQM result for $|Q^2 F_{\eta_b\gamma}(Q^2)|$ shows the asymptotic behavior for high $|Q^2|$ values, but again the result in the spacelike region reaches the asymptotic value faster than that in the timelike region.

In Fig. 6, we show the contributions of the leading- and higher-twist DAs to the transition form factors $Q^2 F_{(\pi,\eta_c,\eta_b)\gamma}(Q^2)$ in the spacelike momentum transfer region ($0 < Q^2 < 100 \text{ GeV}^2$). The dotted, dashed, and dot-dashed lines represent the contributions from the twist-2 DAs $\phi_{2,M}(x)$, the twist-3 DAs $\phi_{3,M}(x)$, and the sum of the twist-2 and twist-3 DAs (see Eq. (10)), respectively. The solid line represents the full results of $Q^2 F_{(\pi,\eta_c,\eta_b)\gamma}(Q^2)$ given by Eq. (3). The results for the heavy quarkonia are obtained from the Set II parameters. As one can see, most of the contributions to $Q^2 F_{\pi\gamma}(Q^2)$ for $Q^2 \geq 10 \text{ GeV}^2$ come from the pion

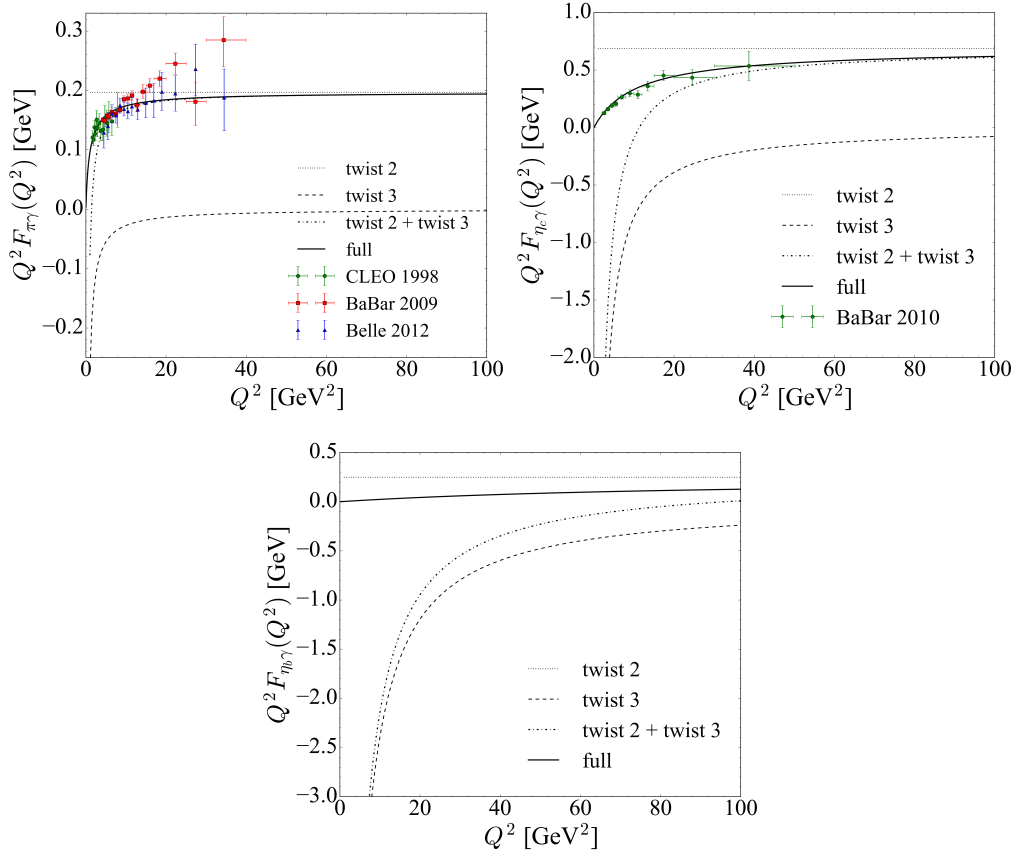


FIG. 6: The contributions of the leading- and higher-twist DAs to the transition form factors $Q^2 F_{(\pi, \eta_c, \eta_b)\gamma}(Q^2)$ in the spacelike momentum transfer region ($0 < Q^2 < 100 \text{ GeV}^2$).

DAs up to twist-3 and the contributions from the twist-4 DAs and above are negligible for $Q^2 \geq 10 \text{ GeV}^2$ region. On the other hand, for the $Q^2 F_{\eta_c\gamma}(Q^2)$ case, the contributions from the twist-2 and twist-3 DAs are dominant only after $Q^2 > 60 \text{ GeV}^2$. This indicates that the higher twist contributions beyond the twist-3 contribution are not negligible to fit the currently available experimental data for $Q^2 F_{\eta_c\gamma}(Q^2)$. For the $Q^2 F_{\eta_b\gamma}(Q^2)$ case, our LFQM shows the necessity of the higher twist contributions beyond the twist-3 contribution even for $Q^2 > 100 \text{ GeV}^2$.

IV. CONCLUSIONS

We studied the $(\eta_c, \eta_b) \rightarrow \gamma^* \gamma$ transitions for the entire kinematic regions analyzing both spacelike and timelike TFFs in our LFQM. Especially, the calculations of $F_{\eta_c\gamma}$ and $F_{\eta_b\gamma}$ have been performed by our newly developed method using the $q^+ \neq 0$ frame with $q^+ = P^+$ [25], which is found to be most effective for the analysis of the timelike region due to the absence of mixing between the internal transverse momentum and the external virtual photon momentum. This leads to the very simple pole structure $1/(q^2 - M_0^2)$ in the form factor, which not only leads to the emergence of the imaginary part of the form factor starting at $q^2 = 4m_Q^2$ ($Q = c, b$) but also provides a straightforward systematic twist expansion of TFFs. We obtained the twist 2 and 3 TMDAs as well as the corresponding twist 2 and 3 DAs in this work using our LFQM framework. As a consistency check for our numerical calculations in timelike region, we have confirmed that our direct LFQM results of $F_{\eta_c(\eta_b)\gamma}(Q^2)$ are in excellent agreement with those obtained from the dispersion relations.

In our numerical calculation of the normalized TFF $F_{\eta_c\gamma}(Q^2)/F_{\eta_c\gamma}(0)$ and the decay width $\Gamma_{\eta_c \rightarrow \gamma\gamma}$, our LFQM results from $m_c = 1.3 \text{ GeV}$ are more consistent with the data [31, 45] than the results from $m_c = 1.8 \text{ GeV}$. Compared to the light pseudoscalar meson TFFs such as $(\pi^0, \eta, \eta') \rightarrow \gamma\gamma^*$ transitions analyzed in [25], the completely symmetric asymptotic behaviors for the heavy $|Q^2 F_{(\eta_c, \eta_b)\gamma}(Q^2)|$ TFFs independent of the timelike and spacelike regions are not reached within a few hundred GeV^2 values of $|Q^2|$. This may be due to the resonance structure occurring at large $q^2 \simeq 4m_Q^2$ ($Q = c, b$) in the timelike region. More elaborate LFQM calculation deserves further study including more trial wave functions such as $2S$ state and even higher excited radial

state harmonic oscillator wave functions.

Acknowledgments

H.-Y. Ryu was supported by the NRF grant funded by the Korea government(MSIP) (No. 2015R1A2A2A01004238). H.-M. Choi was supported by the National Research Foundation of Korea (NRF) (Grant No. NRF-2017R1D1A1B03033129). C.-R. Ji was supported in part by the US Department of Energy (Grant No. DE-FG02-03ER41260).

-
- [1] H.-J. Behrend *et al.* (CELLO Collaboration), Z. Phys. C **49**, 401 (1991).
 - [2] J. Gronberg *et al.* (CLEO Collaboration), Phys. Rev. D **57**, 33 (1998).
 - [3] A. Denig (BESIII Collaboration), Nucl. Part. Phys. Proc. **260**, 79 (2015).
 - [4] S. Uehara *et al.* (Belle Collaboration), Phys. Rev. D **86**, 092007 (2012).
 - [5] B. Aubert *et al.* (BABAR Collaboration), Phys. Rev. D **80**, 052002 (2009).
 - [6] P. del Amo Sanchez *et al.* (BABAR Collaboration), Phys. Rev. D **84**, 052001 (2011).
 - [7] G.P. Lepage and S.J. Brodsky, Phys. Rev. D **22**, 2157 (1980).
 - [8] A. V. Efremov and A. V. Radyushkin, Phys. Lett. B **94**, 245 (1980).
 - [9] V. L. Chernyak and A. R. Zhitnitsky, Phys. Rep. **112**, 173 (1984).
 - [10] S. V. Mikhailov and N. G. Stefanis, Nucl. Phys. B **821**, 291 (2009).
 - [11] A. V. Radyushkin, Phys. Rev. D **80**, 094009 (2009).
 - [12] M. V. Polyakov, JETP Lett. **90**, 228 (2009).
 - [13] A. E. Dorokhov and E. A. Kuraev, Phys. Rev. D **88**, 014038 (2013).
 - [14] X.-G. Wu and T. Huang, Phys. Rev. D **82**, 034024 (2010).
 - [15] P. Kroll, Eur. Phys. J. C **71**, 1623 (2011).
 - [16] S. S. Agaev, V. M. Braun, N. Offen and F. A. Porkert, Phys. Rev. D **86**, 077504 (2012).
 - [17] H. L. L. Roberts, C. D. Roberts, A. Bashir, L. X. Gutiérrez-Guerrero, and P. C. Tandy, Phys. Rev. C **82**, 065202 (2010).
 - [18] S.J. Brodsky, F.-G. Cao, and Guy F. de T ramond, Phys. Rev. D **84**, 075012 (2011).
 - [19] N. G. Stefanis, A. P. Bakulev, S. V. Mikhailov, and A. V. Pimikov, Phys. Rev. D **87**, 094025 (2013).
 - [20] W. Lucha and D. Melikhov, J. Phys. G **39**, 045003 (2012).
 - [21] J. P. B. C. de Melo, B. El-Bennich, and T. Frederico, Few Body Syst. **55**, 373 (2014).
 - [22] S. S. Agaev, V. M. Braun, N. Offen, F.A. Porkert and A. Sch fer, Phys. Rev. D **90**, 074019 (2014).
 - [23] R. Escribano, P. Masjuan and P. Sanchez-Puertas, Eur. Phys. J. C **75**, 414 (2015).
 - [24] R. Escribano, S. Gonz lez-Sol s, P. Masjuan and P. Sanchez-Puertas, Phys. Rev. D **94**, 054033 (2016).
 - [25] H.-M. Choi, H.-Y. Ryu and C.-R. Ji, Phys. Rev. D **96**, 056008 (2017).
 - [26] H.-M. Choi and C.-R. Ji, Phys. Rev. D **59**, 074015 (1999).
 - [27] H.-M. Choi and C.-R. Ji, Phys. Rev. D **75**, 034019 (2007).
 - [28] H.-M. Choi and C.-R. Ji, Phys. Lett. B **460**, 461 (1999).
 - [29] H.-M. Choi, Phys. Rev. D **75**, 073016 (2007).
 - [30] H.-M. Choi and C.-R. Ji, Phys. Rev. D **80**, 054016 (2009).
 - [31] J. P. Lees *et al.* (BABAR Collaboration), Phys. Rev. D **81**, 052010 (2010).
 - [32] T. Feldmann and P. Kroll, Phys. Lett. B **413**, 410 (1997).
 - [33] F. G. Cao and T. Huang, Phys. Rev. D **59**, 093004 (1999).
 - [34] J. J. Dudek and R. G. Edwards, Phys. Rev. Lett. **97**, 172001 (2006).
 - [35] T. Chen *et al.* (CLQCD Collaboration), Eur. Phys. J. C **76**, 358 (2016).
 - [36] F. Feng, Y. Jia and W.-L. Sang, Phys. Rev. Lett. **115**, 222001 (2015).
 - [37] S. Q. Wang, X. G. Wu, W.-L. Sang and S. J. Brodsky Phys. Rev. D **97**, 0094034 (2018).
 - [38] W. Lucha and D. Melikhov, Phys. Rev. D **86**, 016001 (2012).
 - [39] C. Q. Geng and C. C. Lih, Eur. Phys. J. C **73**, 2505 (2013).
 - [40] J. Chen, M. Ding, L. Chang, and Y.-X. Liu, Phys. Rev. D **95**, 016010 (2017).
 - [41] H.-M. Choi and C.-R. Ji, Phys. Rev. D **91**, 014018 (2015).
 - [42] H.-M. Choi and C.-R. Ji, Phys. Rev. D **89**, 033011 (2014).
 - [43] H.-M. Choi and C.-R. Ji, Phys. Rev. D **95**, 056002 (2017).
 - [44] K. W. Edwards *et al.* (CLEO Collaboration), Phys. Rev. Lett. **86**, 30 (2001).
 - [45] M. Tanabashi *et al.* (Particle Data Group), Phys. Rev. D **98**, 030001 (2018).